Random Raman Fiber Laser as a Liquid Refractive Index Sensor

Bing HAN[1,2], Yuxi MA[1,2], Han WU[3*], and Yong ZHAO[1,2*]

[1]*College of Information Science and Engineering, Northeastern University, Shenyang 110819, China*

[2]*Hebei Key Laboratory of Micro-Nano Precision Optical Sensing and Measurement Technology, Qinhuangdao 066004, China*

[3]*College of Electronics and Information Engineering, Sichuan University, Chengdu 610064, China*

[*]Corresponding authors: Han WU and Yong ZHAO   E-mail: hanwu@scu.edu.cn and zhaoyong@ise.neu.edu.cn

Abstract: In this paper, a new concept of forward-pumped random Raman fiber laser (RRFL)-based liquid refractive index sensing is proposed for the first time. For liquid refractive index sensing, the flat fiber end immersed in the liquid can act as the point reflector for generating random fiber lasing and also as the sensing head. Due to the high sensitivity of the output power of the RRFL to the reflectivity provided by the point reflector in the ultralow reflectivity regime, the proposed RRFL is capable of achieving liquid refractive index sensing by measuring the random lasing output power. We theoretically investigate the effects of the operating pump power and fiber length on the refractive index sensitivity for the proposed RRFL. As a proof-of-concept demonstration, we experimentally realize high-sensitivity half-open short-cavity RRFL-based liquid refractive index sensing with the maximum sensitivity and the sensing resolution of $-39.88\,\text{W/RIU}$ and $2.5075 \times 10^{-5}\,\text{RIU}$, respectively. We also experimentally verify that the refractive index sensitivity can be enhanced with the shorter fiber length of the RRFL. This work extends the application of the random fiber laser as a new platform for highly-sensitive refractive index sensing in chemical, biomedical, and environmental monitoring applications, etc.

Keywords: Fiber optic sensors; refractive index measurements; fiber lasers; Rayleigh scattering; stimulated Raman scattering

1. Introduction

A refractive index is a crucial parameter for materials, such as liquids, crystals, polymers, mammalian tissues, and thin films. The fiber optical liquid refractive index sensing technology, possessing practical merits of immunity to electromagnetic interference, high sensitivity, simple structure, and capability of achieving both single-point sensing and distributed sensing, has been widely used in biomedical therapy, diagnosis, chemical and environmental monitoring applications, etc. [1–3]. Various fiber optical liquid refractive index sensors have been developed based on the refractive index-sensitive micro-structure, such as interferometers [4, 5], fiber gratings [6, 7], and

surface plasmon resonance sensors [8, 9]. However, the used highly-sensitive sensing heads are generally fragile and complex to be fabricated. The cross-sensitivity of the refractive index and other parameters, such as temperature, strain, and vibration, is also a problem for such sensing heads. Besides, the wavelength-based demodulation method is utilized in most of the existing fiber optic liquid refractive index sensors, which requires the broadband and high-resolution optical spectrum analyzer [10–12].

In recent years, a new kind of fiber lasers, which is named as random fiber laser (RFL), with random feedback induced by distributed Rayleigh backscattering in the long passive fiber, or random fiber gratings, instead of the conventional oscillation resonator, has attracted plenty of attention [13–15]. RFLs with the merits of low noise [16, 17], flexible wavelength [18, 19], high power [20, 21], etc., have found applications in temporal ghost imaging [22], pulse generation [23], mid-infrared lasers [24], nonlinear frequency conversion [25, 26], etc. One of the most imperative application scenarios of RFLs is optical fiber sensing. Regarding RFLs based on random fiber gratings, the random fiber gratings, which are sensitive to temperature and strain parameters, can also serve as the sensing head and modulate the lasing wavelengths [27–29]. In addition, RFL sensors are also capable of acoustic signal detection with the reduced thermal frequency noise and high resolution [30–32].

Random Raman fiber lasers (RRFLs), based on the feedback and gain provided by Rayleigh backscattering and stimulated Raman scattering (SRS) along the passive fiber, respectively, show the good temporal stability and intrinsic long cavity characteristics. RRFLs can be utilized as amplification pump sources to extend detection ranges in distributed optical fiber sensing systems [33]. In addition, backward-pumped RRFLs that are insensitive to the temperature variation [34] provide unique solutions to realize long-distance remote

sensing. For the backward-pumped RRFL with fiber Bragg gratings (FBGs) or interferometers at the far end of the fiber, the wavelength of random lasing is determined by sensing parameters applied on utilized FBGs or interferometers. Therefore, the generated random lasing can act as the sensing signal to achieve temperature and static or dynamic strain detection with the high optical signal-to-noise ratio (OSNR) [34–37]. Recently, a 200 km-long 6th-order RRFL remote sensing system adopting the ultra-low-loss fiber and erbium-doped fiber is demonstrated with the OSNR of the four FBGs placed at the end of the fiber higher than 15 dB [37]. However, the existing backward-pumped RRFL-based sensing systems need to employ FBGs or interferometers as the sensing head, and the capability of liquid refractive index sensing has not been demonstrated.

Forward-pumped RRFLs have been generally demonstrated for power scaling with the merit of high-efficiency output [38, 39]. With the low reflectivity of the point reflector, the random Raman lasing stimulated threshold is highly related to the reflectivity of the point reflector [40]. Meanwhile, the reflectivity provided by the fiber flat end is negatively correlated with the refractive index of the medium. Hence, the forward-pumped RRFL with the fiber flat end as the point reflector would be a good candidate for liquid refractive index sensing. However, the refractive index sensing ability of the forward-pumped RRFL still remains untapped.

In this paper, a novel concept of realizing liquid refractive index sensing based on a forward-pumped RRFL with the fiber flat end immersed in the liquid as the point reflector is proposed. The power performances of the forward-pumped RRFL according to the liquid refractive index are theoretically investigated. Simulation results show that both the lasing generation threshold and output power are sensitive to the refractive index in the forward-pumped short-cavity RRFL. As a proof-of-concept demonstration, a forward-pumped

500 m-long short-cavity RRFL-based liquid refractive index sensor, which is formed by a 1090 nm pump source and a fiber flat end as the sensing head, is experimentally demonstrated with a maximum sensitivity of −39.88 W/RIU. We also experimentally verify that the refractive index sensitivity can be enhanced with the shorter fiber length of the RRFL.

2. Operation principles

We first theoretically study the power characteristics of the random fiber lasing in the forward-pumped RRFL formed by the point reflector with different reflectivities in a short cavity based on the power balanced model [41]. In the simulations, the wavelengths are set to be 1090 nm and 1145 nm for the pump and the 1st-order random lasing, respectively. A 500 m-long dispersion shifted fiber (DSF), which has the higher nonlinearity than the standard single-mode fiber, is considered as the transmission fiber here, to decrease the lasing generation threshold. It is worth mentioning that the random Raman lasing threshold in the half-open cavity is insensitive to the reflectivity provided by the point reflector when the reflectivity is relatively high, which has been studied in [40]. Hence, we investigate the power characteristics of half-open cavity random Raman lasing with the ultralow reflection at the pump side. According to the Fresnel formulas, the reflectivities of the fiber flat end placed in air and water are 3.38% and 0.18%, respectively. As illustrated in Fig. 1(a), with the forward reflectivity for the random Raman lasing increasing from 0.1% to 4%, the lasing threshold power reduces from 11.5 W to 9 W. Meanwhile, by fixing the pump power to be 11.67 W, the random lasing output power in the forward-pumped structure with different reflectivities at the pump side is calculated. When the reflectivity increases from 0.1% to 4%, the stimulated random Raman lasing power increases from 0.3 W to 7.69 W, as illustrated in Fig. 1(b). For the forward-pumped RRFL, the

lasing threshold and the output power are obviously different from those of the fiber flat end at the pump side placing in air and water, which shows a potential for liquid refractive index sensing based on the RRFL.
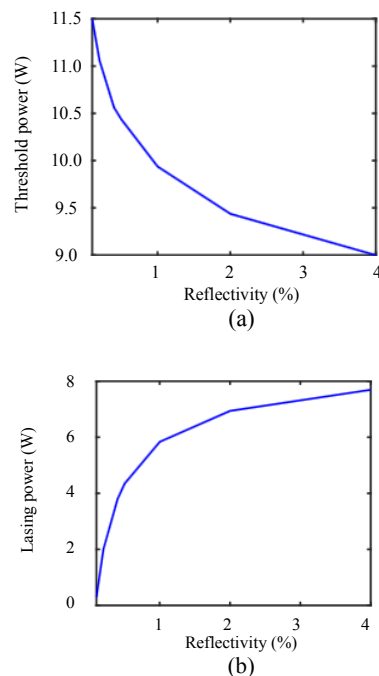

Fig. 1 Simulation results of the forward-pumped RRFL: (a) generation threshold and (b) output power at 11.67 W pump power versus the point reflector reflectivity.

The capability of the forward-pumped RRFL employing the fiber flat end for liquid refractive index sensing is then analyzed theoretically. The lasing threshold of the 500 m-long forward-pumped RRFL is calculated and plotted in Fig. 2(a), considering the fiber flat end immersed in the aqueous solutions with the refractive index rising from 1.3330 to 1.3800. With the increment of the liquid refractive index, the reflectivity of the fiber flat end decreases correspondingly, which results in the higher threshold of the random Raman lasing. Then, Fig. 2(b) shows that by fixing the pump power to be 12 W, the random lasing power changes from 2.70 W to 0.29 W with the increment of the refractive index from 1.3330 to 1.3800. In the reflectivity variation range for the liquid refractive index sensing, the relationship between the output

lasing power and refractive index can be linearly fitted with a linear fitting coefficient as 0.9988, which is plotted in Fig. 2(b). The liquid refractive index sensitivity of the 500 m-long RRFL at the 12 W pump power is as high as -50.74 W/RIU. Figure 2(c) illustrates that with the pump power raised to 14 W, the 1st-order random lasing power varies less to the refractive index at the fiber flat end, but still maintaining a relatively high sensitivity of -49.47 W/RIU. In addition, the linear fitting coefficient of the random Raman lasing power and the refractive index at the fiber flat end is 0.9914.
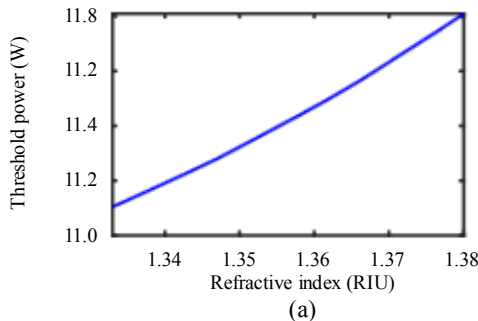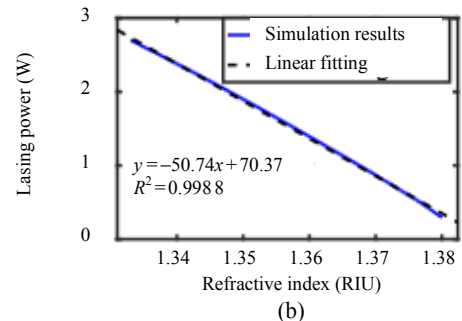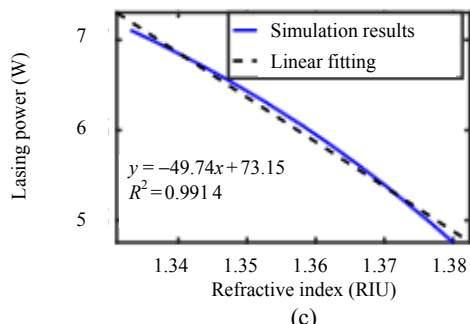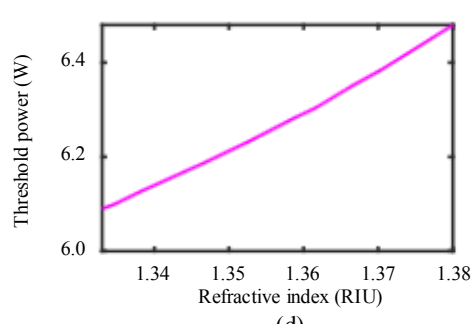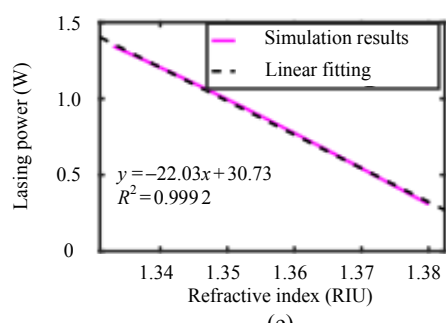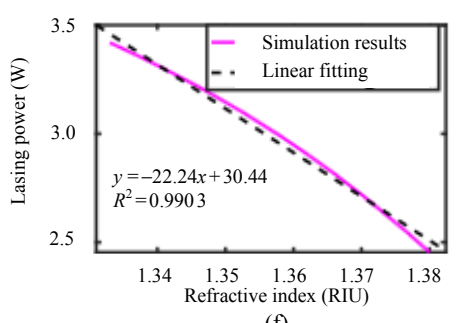

Fig. 2 Numerical calculated results of the forward-pumped RRFL versus the refractive index at the fiber flat end: (a) generation threshold, (b) lasing power at the 12 W pump power, and (c) lasing power at the 14 W pump power of the 500 m-long RRFL; (d) threshold power, (e) lasing power at 6.65 W pump power, and (f) lasing power at 8 W pump power of the 1 km-long RRFL.

To further verify the impact of the forward-pumped RRFL cavity length on the sensing performance, Figs. 2(d), 2(e), and 2(f) show the simulated lasing thresholds and output power for the 1 km-long RRFL at the 6.65 W and 8 W pump power, respectively. By extending the cavity length in the forward-pumped RRFL, the lasing threshold is effectively reduced. However, the refractive index sensitivity is only -22.03 W/RIU for 1 km-long cavity at the 6.65 W pump power, due to the reduction of the lasing efficiency. In addition, it shows a further reduction to -20.24 W/RIU at the 8 W pump power. The results illustrate that the forward-pumped RRFL is a good candidate for

high-performance realizing liquid refractive index sensing with the simple and robust sensing head, which can be a fiber flat end. Besides, the use of the shorter cavity length could help to achieve the higher refractive index sensitivity for the RRFL-based liquid refractive index sensor.

3. Experimental setup and results

The schematic diagram of the proposed forward-pumped half-open cavity RRFL-based liquid refractive index sensor is plotted in Fig. 3. An amplified ytterbium-doped random fiber lasing source as shown in [42] is used as the pump in this paper and launches into the DSF via the pass port (1 040 nm–1 090 nm) of a wavelength division multiplexer (WDM). A flat-end fiber is connected to the reflection port (1 100 nm–1 700 nm) of the WDM to form a forward-pumped RRFL assisted by the Rayleigh backscattering feedback and SRS gain along the DSF in a half-open cavity. The fiber flat end is located in air or immersed in aqueous solutions with different refractive indices. A 1:99 optical coupler (OC) is employed to simultaneously monitor the lasing spectra and output power of the RRFL. To separate the random lasing and the residual pump light, another WDM with the same parameters is inserted between the DSF and the OC, as shown in the dashed box in Fig. 3. All the fiber ends, except the fiber flat end at the pump side, are angle-cleaved.
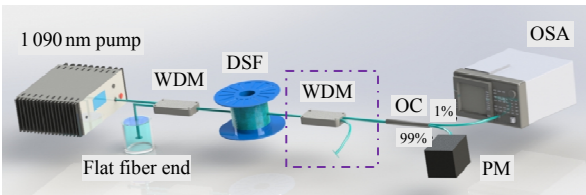

Fig. 3 Schematic diagram of the forward-pumped RRFL-based liquid refractive index sensor. PM: power meter; OSA: optical spectrum analyzer.

Figures 4(a) and 4(b) depict the lasing spectra of the forward-pumped half-open cavity RRFL with the fiber flat end placed in air and pure water at different pump power, which are measured directly after the DSF, respectively. Based on the 1 090 nm pump, the wavelength of the generated random lasing is 1 145 nm. As the reflectivity at the fiber flat end placed in air is higher than that in pure water, the random Raman lasing is stimulated at the lower pump power with the fiber flat end placed in air. Figure 4(c), which is the random lasing power versus the pump power, illustrates that the random lasing generation thresholds with the fiber flat end placed in air and pure water are 10.45 W and 11.73 W, respectively. The random lasing power grows rapidly with the slope efficiency of > 300%, right after the pump power crossing threshold. Finally, the 1st-order random lasing power with the fiber flat end placed in air is 2.96 W higher than that in pure water at the 13.5 W pump power.
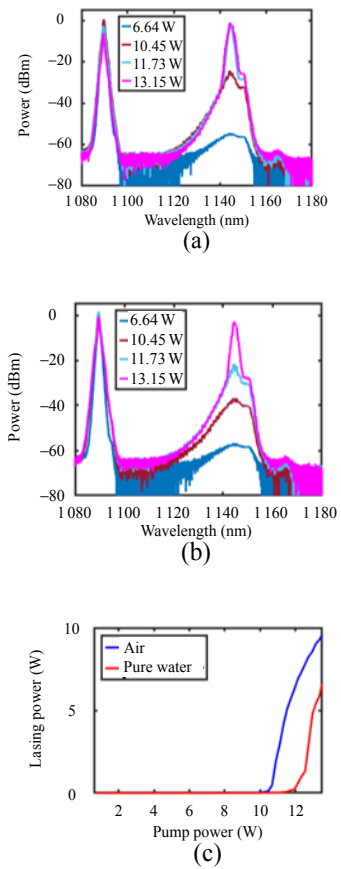

Fig. 4 Lasing spectra of the RRFL based on 500 m DSF with the fiber flat end placed in (a) air and (b) pure water, respectively; (c) 1st-order random lasing power conversion versus 1 090 nm pump power.

In this work, the stimulated random lasing power is monitored to realize liquid refractive index

sensing. The proposed sensing method requires a high spectral purity of the random lasing to avoid the impact of the residual pump power. The low spectral purity of random lasing would affect the refractive index sensing result and lead to the worse accuracy. Therefore, a WDM is inserted between the end of the DSF and the 1:99 OC to divide the residual pump and the random lasing. By immerging the fiber flat end in aqueous solutions with different refractive indices induced by different sodium chloride contents, the measured 1st-order random lasing power varies correspondingly as the blue stars depicted in Fig. 5(a). Due to the existence of stimulated Brillouin scattering for the RRFL at the pump power near the threshold, the fluctuation of the stimulated lasing power could be severe [12]. In the practical experiments, a little bit higher pump power would be more proper to meet the requirement of both high sensitivity and good power stability. The measured 1st-order random lasing power is 4.398 W, at 13.15 W pump power, with the fiber flat end placed in pure water with the refractive index of 1.333 0. Then, the random lasing power drops to 2.589 W, by adding the sodium chloride concentration to increase the aqueous solution refractive index to 1.377 0. The output power of the 1st-order RRFL versus liquid refractive index shows a good linear relationship with R^2 of 0.991 5, which is plotted by the dashed line in Fig. 5(a). The sensitivity of the proposed 500 m-long forward-pumped RRFL-based liquid refractive index sensor at the pump power of 13.15 W is −39.88 W/RIU. The power resolution of the power meter used in this work is 1 mW, so the sensing resolution of the 500 m-long RRFL-based liquid refractive index sensor is 2.5075×10^{-5} RIU. In addition, in Fig. 5(a), the red line illustrates the theoretically calculated power variation versus the refractive index. The insert loss of the WDM is accounted in the theoretical calculations. The experimental result shows the good consistency with the simulation result. As illustrated in Fig. 5(b), the measured lasing power shows a linear relationship to the aqueous solution refractive index increment with R^2 of 0.990 9, by rising the pump power to 13.5 W. Meanwhile, the refractive index sensitivity decreases to −37.03 W/RIU with the corresponding sensing resolution as 2.7005×10^{-5} RIU. The results prove that the proposed sensing method based on the forward-pumped cavity RRFL is effective. The difference between the measured and the calculated refractive index sensing sensitivity shown in Figs. 2 and 5 is caused by the different applied pump powers. Because the stimulated random lasing is unstable right above the generation threshold, the pump power used in the experiments is higher than the considered in the numerical calculation, resulting in a lower refractive index sensing sensitivity. It is worth mentioning that, since the fiber flat end reflectivity is insensitive to the environmental temperature, strain, or vibration, the problem of cross-sensitivity of the refractive index and other sensing parameters could be avoided in the proposed RRFL-based liquid refractive index sensor.

Then, the power stability of the 500 m-long half-open cavity RRFL is investigated in a 10 mins span. Near the lasing generation threshold, the intensity fluctuation is severe as plotted in Fig. 6(a). The output lasing power is 0.840 W with the peak-to-peak power variation of 0.042 W at the 12.34 W pump power, making the measurement accuracy restricted. The power variation of the RRFL at the 13.15 W pump power is ±0.010 W with the average power of 4.398 W, which can be seen in Fig. 6(b). Similar lasing power variation of the 5.366 W random lasing, by increasing the pump power to 13.5 W, is observed in Fig. 6(c). The measurement results verify that the accuracy of the refractive index can be ensured in our scheme and the proper operating pump power should be chosen to balance the temporal stability and refractive index sensitivity.
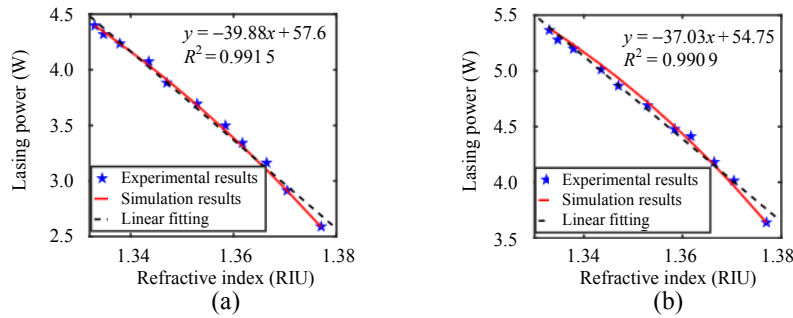
Fig. 5 Liquid refractive index sensing results of the 500 m-long half-open cavity RRFL sensor at (a) 13.15 W and (b) 13.5 W pump power, respectively.
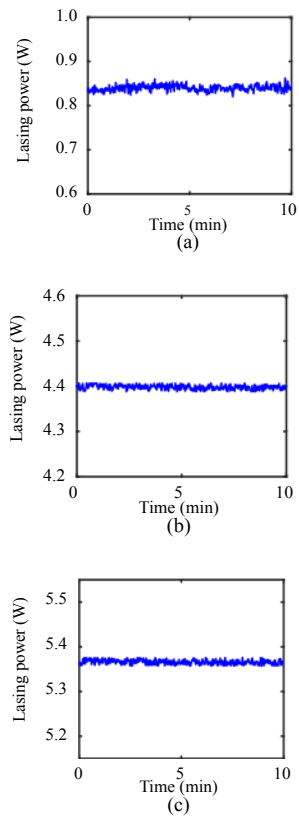

Fig. 6 First-order random lasing power stability in the 500 m-long RRFL with the fiber flat end placed in pure water at (a) 12.34 W, (b) 13.15 W, and (c) 13.5 W pump power, respectively.

To further investigate the impact of the cavity length on the performances in the proposed sensing method, the performances of the forward-pumped RRFL-based liquid refractive index sensor with 1 km-long DSF are investigated as well. As depicted in Fig. 7(a), the lasing spectra of the 1 km-long forward-pumped RRFL with the fiber flat end

placed in pure water at different pump power are measured at first. The threshold is 6.64 W for the RRFL with the fiber flat end placed in pure water. In the measured lasing spectrum for the RRFL with the fiber flat end placed in pure water at 6.64 W, random spikes can be observed caused by the cascaded stimulated Brillouin scattering. The spectrum becomes stable until the pump power increases to 8.14 W. Then, the liquid refractive index sensing performances of the 1 km-long half-open cavity RRFL at the pump power of 8.14 W are measured as well. With the refractive index increasing from 1.333 0 to 1.377 0, the random lasing power decreases from 2.766 W to 2.082 W correspondingly, as plotted in the blue stars in Fig. 7(b). The simulation results, which are illustrated as the red line in Fig. 7(b), show the good consistency with the experimental results. The linear fitting coefficient of the sensing results is 0.994 0. With the lower conversion efficiency in the longer cavity RRFL, the refractive index sensitivity of the 1 km-long RRFL is only -15.58 W/RIU with the sensing resolution of $6.418\,5 \times 10^{-5}$ RIU. Figure 7(c) shows the measured long-term 1st-order random lasing power stability with the output power of 2.766 W at the 8.14 W pump power in the 1 km-long DSF. The lasing power variation at the 8.14 W pump power is ± 0.012 W. The results indicate that the sensing performances in the aspects of the sensitivity and resolution of the proposed forward-pumped RRFL-based liquid refractive index sensor can be

further enhanced by employing the shorter cavity fiber length.
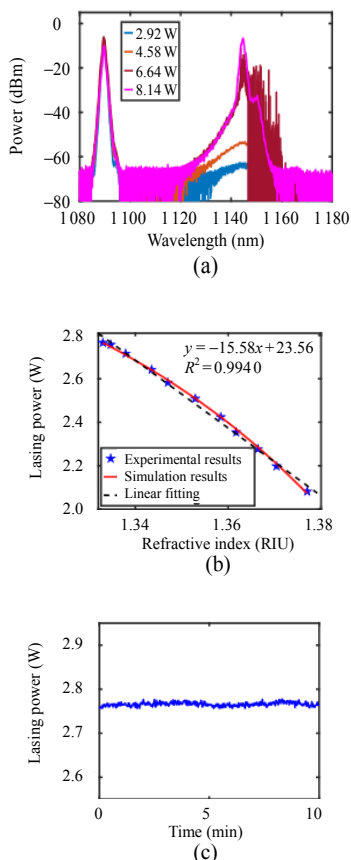
Fig. 7 Experimental results of the 1 km-long RRFL-based liquid refractive index sensor: (a) lasing spectra of the RRFL with the flat-end fiber placed in pure water, (b) sensing results at the 8.14 W pump power, and (c) power stability of the RRFL with the flat-end fiber placed in pure water at the 8.14 W pump power.

4. Conclusions

In this paper, a novel liquid refractive index sensing method based on the forward-pumped RRFL is proposed. The power characteristics and refractive sensing capability of the forward-pumped RRFL with the fiber flat end as a point reflector are investigated theoretically and experimentally. By adopting the 500 m-long RRFL with a fiber flat end as the sensing head, a liquid refractive index sensing system with the sensitivity and sensing resolution of −39.88 W/RIU and 2.5075×10^{-5} RIU, respectively, is experimentally demonstrated. The refractive index sensing behaviors of the RRFL at different operating

pump power and cavity lengths are studied as well. We verify that the shorter cavity length attributes to the higher sensing sensitivity and resolution. The proposed liquid refractive index sensing method based on the forward-pumped RRFL provides a new platform for biomedical therapy, diagnosis, chemical and environmental monitoring applications, etc.

Acknowledgment

Declarations

References

[1] Y. Qian, Y. Zhao, Q. Wu, and Y. Yang, "Review of salinity measurement technology based on optical fiber sensor," *Sensors and Actuators B: Chemical*, 2018, 260: 86–105.

[2] Y. Xu, P. Bai, X. Zhou, Y. Akimov, C. E. Png, L. Ang, *et al.*, "Optical refractive index sensors with plasmonic and photonic structures: promising and inconvenient truth," *Advanced Optical Materials*, 2019, 7(9): 1801433.

[3] Z. Ding, K. Sun, K. Liu, J. Jiang, D. Yang, Z. Yu, *et al.*, "Distributed refractive index sensing based on tapered fibers in optical frequency domain reflectometry," *Optics Express*, 2018, 26(10): 13042–13054.

[4] R. Fan, Q. Ma, L. Li, Y. Zhuo, J. Shen, Z. Ren, *et al.*, "Liquid level and refractive index double-parameter

sensor based on tapered photonic crystal fiber," *Journal of Lightwave Technology*, 2020, 38(14): 3717–3722.

[5] D. Aydin, J. A. Barnes, and H. Loock, "In-fiber interferometry sensors for refractive index," *Applied Physics Reviews*, 2023, 10(1): 011307.

[6] J. Albert, L. Shao, and C. Caucheteur, "Tilted fiber Bragg grating sensors," *Laser & Photonics Reviews*, 2013, 7(1): 83–108.

[7] H. Li, J. Liu, X. He, J. Yuan, Q. Wu, and B. Liu, "Long-period fiber grating based on side-polished optical fiber and its sensing application," *IEEE Transactions on Instrumentation and Measurement*, 2023, 72: 7001109.

[8] C. Liu, J. Lv, W. Liu, F. Wang, and P. K. Chu, "Overview of refractive index sensors comprising photonic crystal fibers based on the surface plasmon resonance effect," *Chinese Optics Letters*, 2021, 19(10): 102202.

[9] L. Li, Y. Zhang, W. Zheng, R. Lv, and Y. Zhao, "Dual-channel in-fiber SPR sensor for simultaneous and highly sensitive measurement of salinity and temperature," *Optics Letters*, 2023, 48(4): 952–955.

[10] C. Holmes, S. Ambran, P. A. Cooper, A. S. Webb, J. C. Gates, C. B. E. Gawith, *et al.*, "Bend monitoring and refractive index sensing using flat fibre and multicore Bragg gratings," *Measurement Science and Technology*, 2020, 31(8): 085203.

[11] Y. Wang, Z. Chen, W. Chen, and X. Zhang, "Refractive index and temperature sensor based on fiber ring laser with tapered seven core fiber structure in 2 μm band," *Optical Fiber Technology*, 2021, 61: 102388.

[12] F. Zhao, W. Lin, J. Hu, S. Liu, F. Yu, X. Chen, *et al.*, "Highly sensitive salinity and temperature measurement based on tapered-SHF MZI fiber laser structure," *Measurement Science and Technology*, 2023, 34(6): 064002.

[13] S. K. Turitsyn, S. A. Babin, A. E. El Taher, P. Harper, D. V. Churkin, S. I. Kablukov, *et al.*, "Random distributed feedback fibre laser," *Nature Photonics*, 2010, 4(4): 231–235.

[14] A. S. L. Gomes, A. L. Moura, C. B. Araújo, and E. P. Raposo, "Recent advances and applications of random lasers and random fiber lasers," *Progress in Quantum Electronics*, 2021, 78: 100343.

[15] D. V. Churkin, S. Sugavanam, I. D. Vatnik, Z. Wang, E. V. Podivilov, S. A. Babin, *et al.*, "Recent advances in fundamentals and applications of random fiber lasers," *Advances in Optics and Photonics*, 2015, 7(3): 516–569.

[16] B. Han, Y. Rao, H. Wu, J. Yao, H. Guan, R. Ma, *et al.*, "Low-noise high-order Raman fiber laser pumped by random lasing," *Optics Letters*, 2020, 45(20): 5804–5807.

[17] R. Deheri, S. Dash, V. R. Supradeepa, and V. Balaswamy, "Cascaded Raman fiber lasers with ultrahigh spectral purity," *Optics Letters*, 2022, 47(14): 3499–3502.

[18] L. Zhang, J. Dong, and Y. Feng, "High-power and high-order random Raman fiber lasers," *IEEE Journal of Selected Topics in Quantum Electronics*, 2018, 24(3): 1400106.

[19] Y. Zhang, J. Ye, X. Ma, J. Xu, J. Song, T. Yao, *et al.*, "High power tunable multiwavelength random fiber laser at 1.3 μm waveband," *Optics Express*, 2021, 29(4): 5516–5524.

[20] H. Zhang, J. Wu, Y. Wan, P. Wang, B. Yang, X. Xi, *et al.*, "Kilowatt random Raman fiber laser with full-open cavity," *Optics Letters*, 2022, 47(3): 493–496.

[21] R. Ma, X. Quan, H. Wu, W. Gao, D. Huang, X. Wang, *et al.*, "20 watt-level single transverse mode narrow linewidth and tunable random fiber laser at 1.5 μm band," *Optics Express*, 2022, 30(16): 28795–28804.

[22] H. Wu, B. Han, Z. Wang, G. Genty, and H. Liang, "Temporal ghost imaging with random fiber lasers," *Optics Express*, 2020, 28(7): 9957–9964.

[23] S. Wang, W. Zhang, Y. Zhang, and Y. Rao, "Raman gain square-wave noise-like pulse laser pumped by a random fiber laser," *Annalen der Physik*, 2021, 533(2): 2000452.

[24] Y. Wang, H. Luo, H. Wu, J. Li, and Y. Liu, "Tunable pulsed dysprosium laser within a continuous range of 545 nm around 3 μm," *Journal of Lightwave Technology*, 2022, 40(14): 4841–4847.

[25] H. Wu, W. Wang, Y. Li, C. Li, J. Yao, Z. Wang, *et al.*, "Difference-frequency generation of random fiber lasers for broadly tunable mid-infrared continuous-wave random lasing generation," *Journal of Lightwave Technology*, 2022, 40(9): 2965–2970.

[26] H. Wu, W. Wang, B. Hu, Y. Li, K. Tian, R. Ma, *et al.*, "Widely tunable continuous-wave visible and mid-infrared light generation based on a dual-wavelength switchable and tunable random Raman fiber laser," *Photonics Research*, 2023, 11(5): 808–816.

[27] J. Deng, D. V. Churkin, Z. Xu, and X. Shu, "Random fiber laser based on a partial-reflection random fiber grating for high temperature sensing," *Optics Letters*, 2021, 46(5): 957–960.

[28] A. Sanchez-Gonzalez, R. A. Perez-Herrera, P. Roldan-Varona, L. Rodriguez-Cobo, J. M. Lopez-Higuera, and M. Lopez-Amo, "High performance fiber laser resonator for dual band (C and L) sensing," *Journal of Lightwave Technology*, 2022, 40(15): 5273–5279.

[29] S. Miao, W. Zhang, W. Huang, and Y. Song, "High-resolution static strain sensor based on random fiber laser and beat frequency interrogation," *IEEE Photonics Technology Letters*, 2019, 31(18): 1530–1533.

[30] Y. Xu, L. Zhang, S. Gao, P. Lu, S. Mihailov, and X.

Bao, "Highly sensitive fiber random-grating-based random laser sensor for ultrasound detection," *Optics Letters*, 2017, 42(7): 1353–1356.

[31] L. Zhang, P. Lu, Z. Zhou, Y. Wang, S. Mihailov, L. Chen, *et al.*, "High-efficiency random fiber laser based on strong random fiber grating for MHz ultrasonic sensing," *IEEE Sensors Journal*, 2020, 20(11): 5885–5892.

[32] Y. Pang, S. Ma, X. Zhao, Z. Qin, Z. Liu, and Y. Xu, "Broadband high-sensitivity acoustic sensing based on Brillouin random fiber laser," *Optics & Laser Technology*, 2023, 161: 109195.

[33] Y. Fu, R. Zhu, B. Han, H. Wu, Y. Rao, C. Lu, *et al.*, "175-km repeaterless BOTDA with hybrid high-order random fiber laser amplification," *Journal of Lightwave Technology*, 2019, 37(18): 4680–4686.

[34] Z. Wang, Y. Rao, H. Wu, P. Li, Y. Jiang, X. Jia, *et al.*, "Long-distance fiber-optic point-sensing systems based on random fiber lasers," *Optics Express*, 2012, 20(16): 17695–17700.

[35] V. M. Soto and M. López-Amo, "Truly remote fiber optic sensor network," *Journal of Physics: Photonics*, 2019, 1: 042002.

[36] S. Lin, Z. Wang, Y. Qi, B. Han, H. Wu, and Y. Rao, "Wideband remote-sensing based on random fiber laser," *Journal of Lightwave Technology*, 2022, 40(9): 3104–3110.

[37] B. Han, H. Wu, Y. Liu, S. Dong, Y. Rao, Z. Wang, *et al.*, "Ultralong single-ended random fiber laser and sensor," *Laser & Photonics Reviews*, 2023, 17: 2200797.

[38] Z. Wang, H. Wu, M. Fan, L. Zhang, Y. Rao, W. Zhang, *et al.*, "High power random fiber laser with short cavity length: theoretical and experimental investigations," *IEEE Journal of Selected Topics in Quantum Electronics*, 2015, 21(1): 0900506.

[39] C. Fan, Y. An, Y. Li, X. Hao, T. Yao, H. Xiao, *et al.*, "Modal dynamics in kilowatt cladding-pumped random distributed feedback Raman fiber laser with brightness enhancement," *Journal of Lightwave Technology*, 2022, 40(19): 6486–6492.

[40] H. Wu, Z. Wang, M. Fan, L. Zhang, W. Zhang, and Y. Rao, "Role of the mirror's reflectivity in forward-pumped random fiber laser," *Optics Express*, 2015, 23(2): 1421–1427.

[41] S. K. Turitsyn, S. A. Babin, D. V. Churkin, I. D. Vatnik, M. Nikulin, and E. V. Podivilov, "Random distributed feedback fibre lasers," *Physics Reports*, 2014, 542: 133–193.

[42] B. Han, S. Dong, Y. Liu, and Z. Wang, "Cascaded random Raman fiber laser with low RIN and wide wavelength tunability," *Photonic Sensors*, 2022, 12(4): 220414.